ELSEVIER

Journal of Power Sources 112 (2002) 419–427

JOURNAL OF POWER SOURCES

www.elsevier.com/locate/jpowsour

On the $Li_xCo_{1-y}Mg_yO_2$ system upon deintercalation: electrochemical, electronic properties and ^7Li MAS NMR studies

S. Levasseur, M. Ménétrier, C. Delmas*

Institut de Chimie de la Matière Condensée de Bordeaux-CNRS and Ecole Nationale Supérieure de Chimie et Physique de Bordeaux, Université Bordeaux I 87, Av. Dr A. Schweitzer, 33608 Pessac Cedex, France

Received 27 May 2002; received in revised form 4 August 2002; accepted 16 August 2002

Abstract

A detailed characterization of the structural modifications and redox processes occurring upon lithium deintercalation from the $Li_{x0}Co_{1-y}Mg_yO_2$ materials ($x_0 = 1.0$ and 1.10; $y = 0.0$, 0.03, 0.05 and 0.06) was performed in order to determine the effect of Mg doping on the cycling properties. Using electrochemical tests, X-ray diffraction (XRD), ^7Li MAS NMR and electrical properties measurements, we show that the $Li_xCo_{1-y}Mg_yO_2$ system exhibits a solid solution existing in the whole deintercalation range studied ($0.30 \leq \times \leq 1.0$). These phases exhibit reversible capacities equivalent to that of $LiCoO_2$ upon cycling with a good structural stability. Moreover, the ^7Li MAS NMR study shows that the structural defects (O vacancies and intermediate spin Co^{3+} ions) which are present in the starting Mg-doped phases govern the electronic properties upon lithium deintercalation. Indeed, regardless of the presence of Mg ions in the structure, a behavior similar to that of the Li_xCoO_2 ($1 < x_0 \leq 1.08$) system is evidenced with an insulator to metal transition taking place at the microscopic scale.

Keywords: $LiCoO_2$; Layered oxide; NMR; Lithium battery; Electrical properties; Magnesium substitution

1. Introduction

Among lithium transition metal oxides used as positive electrode materials for Li-ion cells, $LiCoO_2$ is considered to be the most stable [1,2]. When prepared at high temperature, it exhibits the ideal layered α-$NaFeO_2$-type framework (S.G. R-3*m*) with an AB CA BC packing of the oxygen layers in which Co and Li ions are ordered in octahedral sites of alternate (1 1 1) planes of the cubic closed-packed oxygen lattice [3]. One of the possible modifications to improve its electrochemical performances is to substitute metal ions for Co in order to stabilize the layered structure upon cycling with or without participation to the redox processes. Substitution with Ni [4–7], Mn [8,9], Cr [10], Al [11,12] or Fe [13] have already been studied. Previous work reported the effect of Mg-doping on the electrochemical properties and on the electrical conductivity of $LiCoO_2$ [14,15]. Very recently, we performed a detailed study of the $LiCo_{1-y}Mg_yO_2$ system, looking at the effects of both Mg-doping and Li overstoichiometry. We confirmed previous results such as the increase in dc conductivity in Mg-doped phases compared to pure $LiCoO_2$ and showed, using ^7Li MAS NMR spectroscopy, the coexistence of various Co oxidation states in all the Mg-doped materials, the Mg substitution always leading to the presence of a structural defect associated to oxygen vacancies and to intermediate spin Co^{3+} ions [16], like in the case of Li-overstoichiometric $Li_{x0}CoO_2$ ($x_0 > 1$) [17]. In the parent $Li(Ni,Mg)O_2$ system, Pouillerie et al. argued that Mg substitution could strongly improve the cycling properties by migration of the Mg^{2+} ions from the Ni layer to the interslab space after the first cycle at high potential thus stabilizing the layered framework of the $LiNiO_2$ structure [18].

Taking into account previous results from our former work [16], we carried out a study of the $Li_xCo_{1-y}Mg_yO_2$ ($y = 0.0$, 0.03, 0.05 and 0.06) system upon cycling. We prepared electrochemically deintercalated $Li_xCo_{1-y}Mg_yO_2$ materials ($x_0 = 1.0$ and 1.10; $y = 0.0$, 0.05 and 0.06) and characterized them using X-ray diffraction (XRD), ^7Li MAS NMR spectroscopy and electrical properties measurements.

2. Experimental

The starting $Li_{x0}Co_{1-y}Mg_yO_2$ materials were prepared from Li_2CO_3, Co_3O_4 and MgC_2O_4 by solid state chemistry as described in [16] (x_0 denotes the nominal Li/(Co + Mg) ratio in the starting mixture).

* Corresponding author. Tel.: +33-5-5684-6296; fax: +33-5-5684-6634.
E-mail address: delmas@icmcb.u-bordeaux.fr (C. Delmas).

0378-7753/02/$ – see front matter
PII: S0378-7753(02)00456-1

Electrochemical measurements were carried out at room temperature (22 °C) with Li//$Li_xCo_{1-y}Mg_yO_2$ cells. The positive electrode consisted of a mixture of 88% by weight of active material, 2% of polytetrafluorethylene (PTFE) and 10% of carbon black. The first series of cells (Li/$LiPF_6$–PC (propylene carbonate)–EC (ethylene carbonate)–DEC (diethylcarbonate)/$Li_xCo_{1-y}Mg_yO_2$ cells, assembled in an argon-filled dry box, was charged at 100 μA cm^{-2} (m_{LiCoO_2} = 30 mg, *C*/160 rate); the second series (Li/$LiClO_4$–PC/$Li_xCo_{1-y}Mg_yO_2$), for long-range cycling, was cycled at 400 μA cm^{-2} (m_{LiCoO_2} = 15 mg, *C*/20 rate). The $Li_xCo_{0.95}Mg_{0.05}O_2$ ($x_0 = 1.0$) deintercalated materials for XRD characterization were recovered in an argon-filled dry box, washed in DMC (dimethylcarbonate) and dried under vacuum. For the electrochemical preparation of partially deintercalated phases for electrical measurements and ^{7}Li MAS NMR, sintered pellets (8 mm in diameter, 600 MPa pressure and thermal treatment at 800 °C for 12 h under oxygen) of the starting material were used as positive electrode, without additive. The cells assembled in an argon-filled dry box were charged at 100 μA cm^{-2} ($m_{Li(Co,Mg)O_2}$ = 180 mg). The deintercalated pellets of $Li_x(Co, Mg)O_2$ materials were washed with DMC (dimethylcarbonate) before characterization.

The XRD patterns of the $Li_xCo_{0.95}Mg_{0.05}O_2$ deintercalated materials were recorded on a Philips PW1820 powder diffractometer using the Cu Kα radiation, in a special air-tight holder under argon atmosphere in order to prevent any reaction with air moisture. Refinements of the cell parameters were performed using the Fullprof program (full-pattern matching mode) with a pseudo-Voigt fitting function [19].

^{7}Li MAS NMR spectra were recorded on a Bruker MSL200 spectrometer at 77.7 MHz, with a standard 4-mm Bruker MAS probe. The samples were mixed with dry silica (typically 50% in weight), in order to facilitate the spinning and improve the field homogeneity, since they may exhibit metallic or paramagnetic properties. The mixture was placed into a 4-mm diameter zirconia rotor in the dry box. For all phases, a Hahn echo sequence ($t_{\pi/2}$–τ_1–t_π–τ_2) was utilized in order to facilitate the phasing of all the signals and of their spinning sidebands and to ensure the observation of possibly very wide signals which would be lost during the receiver dead time in single pulse experiments. The 90° pulse duration used ($t_{\pi/2}$) was equal to 3.05 μs. In order to synchronize the spin echo with the first rotational echo, τ_1 was fixed to the rotor period $T_r = 1/\nu_r$. The spinning speed (ν_r) was 15 kHz. A 200-kHz spectral width was used, and the recycle time $D_0 = 1$ s is long enough to avoid T_1 saturation effects. The isotropic shifts reported in parts per million are relative to an external sample of 1 M LiCl solution in water.

Electronic conductivity measurements were carried out on sintered pellets (8 mm in diameter, 600 MPa pressure and thermal treatment at 800 °C for 12 h under oxygen) with the four probe direct current method in the 100–300 K range. Thermoelectronic power measurements were performed with a home-made equipment [20].

3. Results and discussion

3.1. Electrochemical study

Fig. 1 shows the first galvanostatic charge curve of Li/$Li_xCo_{1-y}Mg_yO_2$ cells ($x_0 = 1.0$; $y = 0.0$ and 0.05) at low rate (J = 100 μA cm^{-2}, $m_{Li(Co,Mg)O_2}$ = 30 mg; *C*/160 rate, 160 h are required to exchange one electron).

As already reported, the charge curve obtained with the pure Li_xCoO_2 ($x_0 = 1.0$) material exhibits both the voltage

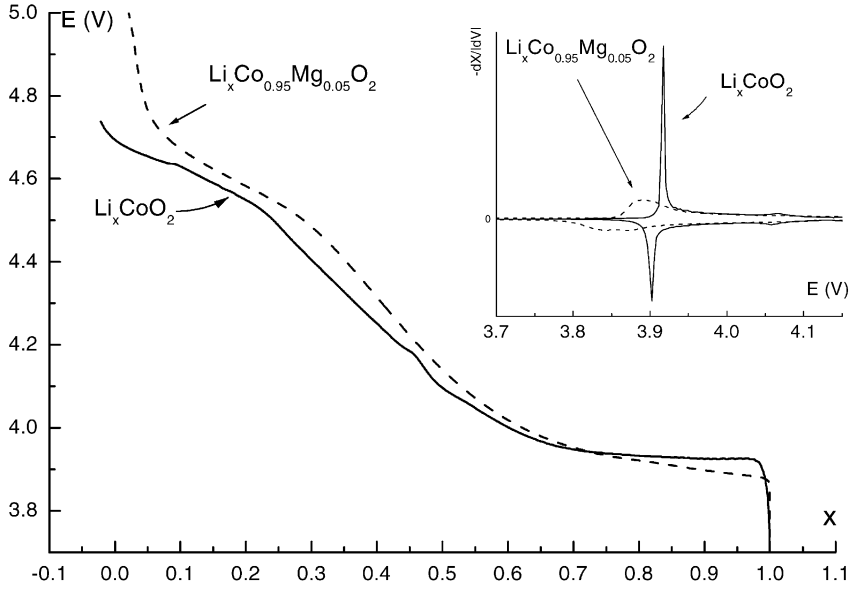

Fig. 1. First galvanostatic charge of Li//$Li_xCo_{1-y}Mg_yO_2$ ($x_0 = 1.0$, $y = 0.0$ and 0.05) electrochemical cells (J = 100 μA cm^{-2}; $m_{Li(Co,Mg)O_2}$ = 30 mg).

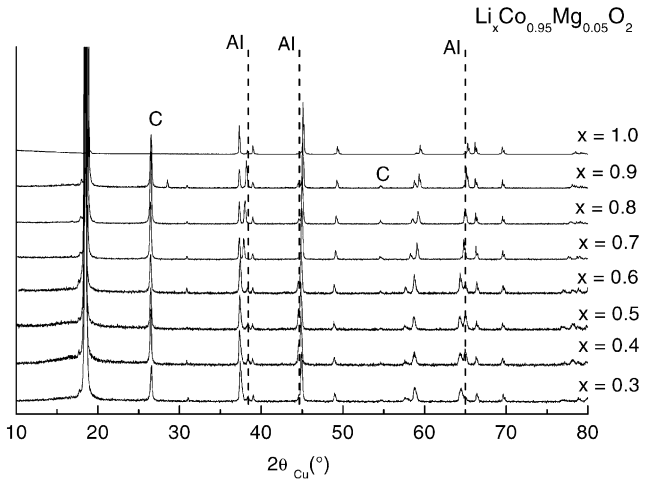

Fig. 2. X-ray diffraction patterns of the electrochemically deintercalated $Li_xCo_{0.95}Mg_{0.05}O_2$ ($x_0 = 1.0$) samples ($0.30 \leq x \leq 1.0$). The C and Al labels show reflections due to carbon added in the electrode and to aluminum from the sample holder, which appears on some of the patterns.

plateau at ca. 3.93 V corresponding to the biphasic domain for $0.75 \leq x \leq 0.94$ due to a macroscopic insulator to metal transition and the particular feature associated to the monoclinic distortion expected for $Li_{0.50}CoO_2$ due to the interslab lithium/vacancy ordering [21–23].

On the contrary, the first galvanostatic charge curve of the Li//$Li_xCo_{0.95}Mg_{0.05}O_2$ ($x_0 = 1.0$) cell shows neither the voltage plateau at the beginning of the charge nor the feature corresponding to the monoclinic distortion for $x = 0.50$. The monotonous increase of the potential during lithium deintercalation suggests the occurrence of a monophasic reaction throughout the charge process for the $Li_xCo_{0.95}Mg_{0.05}O_2$ materials. An XRD study of electrochemically deintercalated $Li_xCo_{0.95}Mg_{0.05}O_2$ ($x_0 = 1.0$) materials confirms such an observation: as shown in Figs. 2 and 3, a solid solution is obtained for $0.30 \leq x \leq 1.0$ in the $Li_xCo_{0.95}Mg_{0.05}O_2$ ($x_0 = 1.0$) system confirming the previous results by Tukamoto and West who showed the existence of a single phase for the $Li_{0.90}Co_{0.95}Mg_{0.05}O_2$ composition [14].

The evolution of the cell parameters during deintercalation in $Li_xCo_{0.95}Mg_{0.05}O_2$ ($x_0 = 1.0$) is shown in Fig. 4 and compared to that obtained in stoichiometric Li_xCoO_2 ($x_0 = 1.0$) [22]. As expected, the c parameter increases due to the increase of the electrostatic repulsion between adjacent oxygen layers, while the a parameter decreases owing to cobalt oxidation.

3.1.1. Discussion on the structural evolution upon charging

Two different reasons can explain the existence of a solid solution upon lithium deintercalation in the $Li_xCo_{0.95}Mg_{0.05}O_2$ ($x_0 = 1.0$) system for $0.30 \leq x \leq 1.0$. Those are as follows.

It is admitted that substitution of an element M for Co in $LiCoO_2$ causes the phase transitions to disappear upon deintercalation (M = Ni [24], Fe [13], Al [12], Mn [9], etc.).

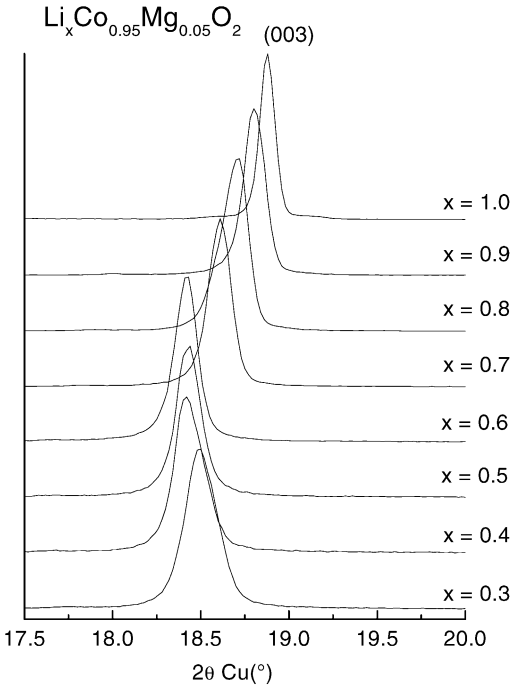

Fig. 3. Expansion of the (0 0 3) Bragg reflection of the X-ray diffraction patterns of electrochemically deintercalated $Li_xCo_{0.95}Mg_{0.05}O_2$ ($x_0 = 1.0$) samples ($0.30 \leq x \leq 1.0$).

This phenomenon is also evidenced in the parent Li(NiM)O_2 system [18,25–31]. Indeed, the M ions substituting for cobalt (nickel respectively) perturb the organization of the metallic cations in the slabs and prevent the rearrangements

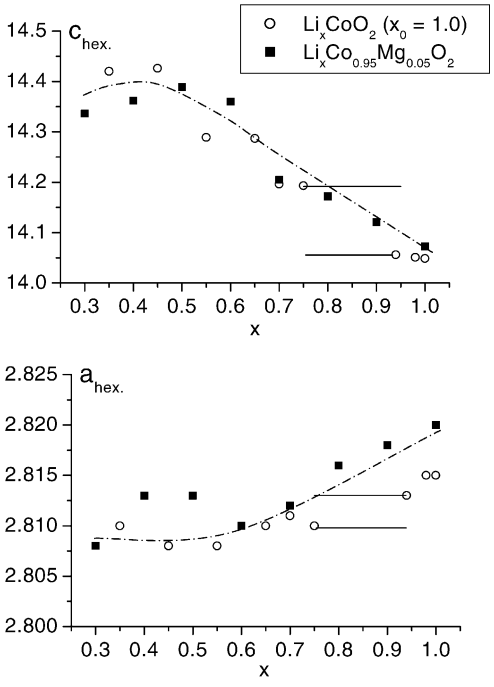

Fig. 4. Evolution of the $a_{hex.}$ and $c_{hex.}$ hexagonal cell parameters as a function of x in the $Li_xCo_{0.95}Mg_{0.05}O_2$ ($x_0 = 1.0$) samples ($0.30 \leq x \leq 1.0$). The evolution for Li_xCoO_2 ($x_0 = 1.0$) is also plotted with a two-phase domain for $0.75 \leq x \leq 0.94$ [22].

of Li^+ ions and electrons that usually occur upon deintercalation in non-substituted systems. Note that in the Li-stoichiometric $Li_xCo_{1-y}Ni_yO_2$ ($x_0 = 1.0$) system, more than 10% of Ni ions are necessary to prevent any phase transition upon lithium deintercalation [7], while in the present case, a very low amount of Mg ions (5%) is sufficient to lead to a solid solution upon charging.

One must take into account the fact that all the $Li_{x0}Co_{1-y}Mg_yO_2$ phases exhibit structural defects related to the presence of intermediate spin Co^{3+} ions (noted $Co^{3+(IS)}$) and of oxygen vacancies, the origin of which has been attributed to the presence of two adjacent Mg^{2+} ions in substitution for Co [16]. Note that these defects suppress all the structural transitions upon deintercalation in the $Li_{1.10}CoO_2$ [32] and $Li_{1.10}Co_{0.97}Ni_{0.03}O_2$ [7] systems.

3.1.2. Cycling tests

Li/$LiClO_4$–PC/$Li_{x0}Co_{1-y}Mg_yO_2$ ($x_0 = 1.0$; $y = 0.0, 0.03, 0.05$ and 0.06) cells were cycled between 2.7 and 4.15 V at 400 μA cm^{-2} (*C*/20 rate) as shown in Fig. 5. The reversible capacity for the first and 10th cycle is also indicated in Fig. 5.

As already reported elsewhere, the cycling behavior of the Mg-doped $Li_xCo_{1-y}Mg_yO_2$ phases is very satisfactory and close to that of pure $LiCoO_2$ [14]. The cycling curves, on Fig. 5, show that the reversibility of the deintercalation/intercalation process is good, as the reversible capacities for the first and 10th cycles, shown in Fig. 5, are rather high in the voltage window used. Note that polarization is very small in all cases and that the irreversible capacity at the first cycle is particularly low.

In addition, Fig. 6 shows the XRD pattern of the $Li_xCo_{0.95}Mg_{0.05}O_2$ material after 60 cycles (*C*/20, between 2.7 and 4.15 V). At the end of the last discharge, a series of relaxation–discharge sequences allowed us to reintercalate as many Li^+ ions as possible (final x close to 0.97). The refinement of the cell parameters shows that the layered structure is stable and that no magnesium ion migrates from the slab to the interslab space, the cell parameters being the same before and after "long-range" cycling. Indeed, in the parent $LiNi_{1-y}Mg_yO_2$ system, the migration of magnesium from the slab to the interslab space during the first cycles leads to an increase of both the $a_{hex.}$ and $c_{hex.}$ parameters, the vacancies created increasing the average Ni–Ni distance in the slab ($LiNi_{0.92}Mg_{0.10}O_2$: $a_{hex.} = 2.8751(2)$ Å, $c_{hex.} = 14.219(2)$ Å; 50 cycled-$Li_xNi_{0.92}Mg_{0.10}O_2$: $a_{hex.} = 2.8816(2)$ Å, $c_{hex.} = 14.236(2)$ Å) [18]. Moreover, one can note that even after cycling, the diffraction lines remain narrow, suggesting that the crystallinity of the material has been retained upon lithium deintercalation/reintercalation, suggesting a good relaxation of the stress induced by the variation of the cell parameters upon cycling. Note that, on Fig. 6, the preferential orientation is rather

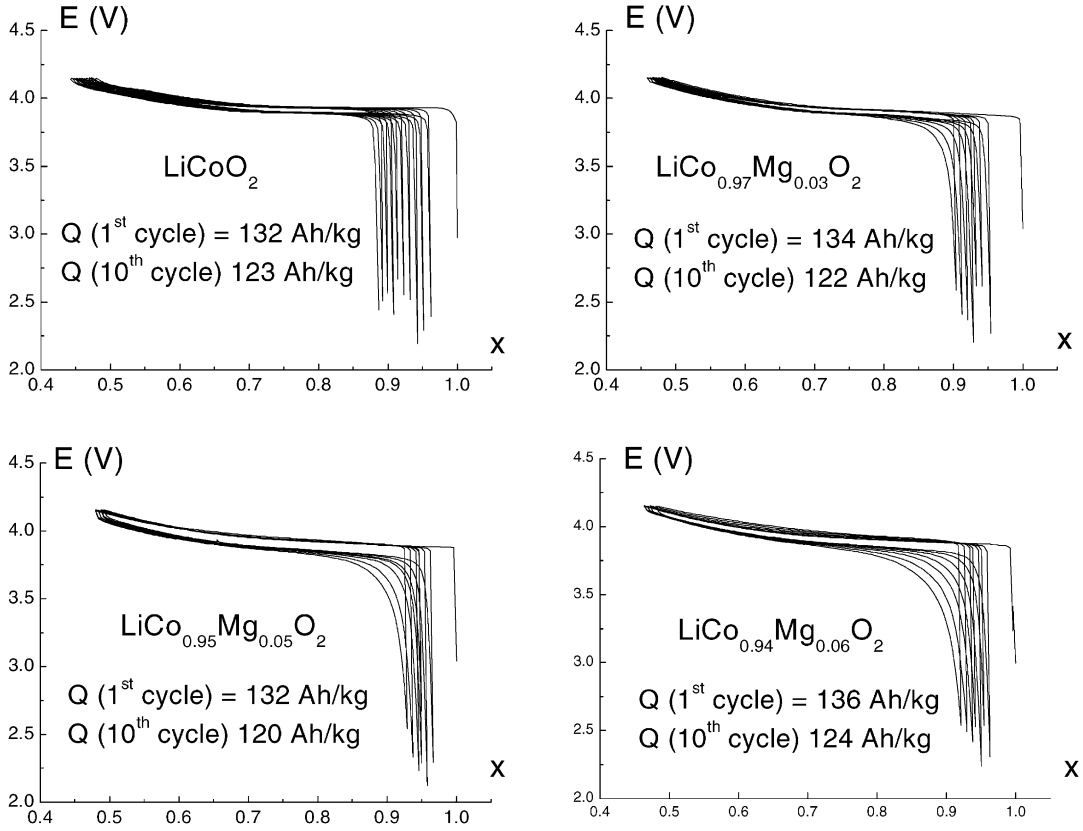

Fig. 5. Cycling behavior of the various Li//$Li_xCo_{1-y}Mg_yO_2$ ($x_0 = 1.0$; $y = 0.0$, 0.03, 0.05 and 0.06) electrochemical cells ($J = 400$ μA cm^{-2}; $m_{Li(Co,Mg)O_2} = 30$ mg, *C*/20 rate) between 2.7 and 4.15 V.

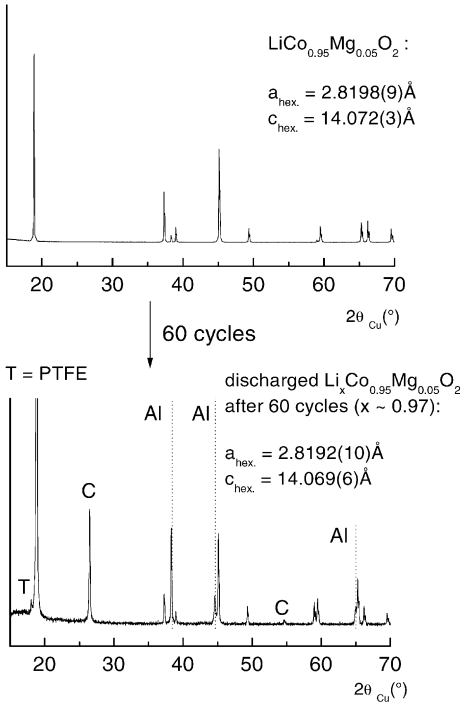

Fig. 6. X-ray diffraction patterns of the $LiCo_{0.95}Mg_{0.05}O_2$ sample before and after 60 cycles. The refined cell parameters are also noted in the figure.

high on the $Li_xCo_{0.95}Mg_{0.05}O_2$ material XRD pattern due to the preparation process of such cycled products, so that no conclusion can be drawn about the line intensity ratios.

3.2. ^{7}Li MAS NMR study

3.2.1. $Li_xCo_{0.94}Mg_{0.06}O_2$ ($x_0 = 1.0$) materials

The ^{7}Li MAS NMR spectra of the various $Li_xCo_{0.94}Mg_{0.06}O_2$ ($x_0 = 1.0$) phases are shown in Figs. 7 and 8, with different scales.

Referring to our previous work on the starting Mg-doped phases, we know that the 55 ppm signal in the NMR spectrum of the $LiCo_{0.94}Mg_{0.06}O_2$ ($x_0 = 1.0$) phase arises from a Knight–Shift type interaction resulting from the presence of itinerant electron holes which induce a pseudo-metallic behavior in the sample at the local scale around one Mg^{2+} ion. In addition to the 55 ppm signal, the two weak signals at 325 and −27 ppm are due to the structural defect leading to the presence of both oxygen vacancies and $Co^{3+(IS)}$ ions. The signal at 325 ppm is related to lithium ions with one $Co^{3+(IS)}$ as first neighbor, the signal at −27 ppm being due to Li^+ ions with $Co^{3+(IS)}$ ions as second neighbor [16].

For $0.85 \leq x \leq 1.0$, like in the case of the non substituted Li_xCoO_2 ($x_0 > 1.0$) system, but in a less marked way, oxidation of cobalt leads to the disappearance of the signals related to the $Co^{3+(IS)}$ ions at 325, 55 and −27 ppm. In the same time, one can observe a continuous decrease of the intensity of the central signal as well as of the 55 ppm signal. This large global decrease of the signal intensity is characteristic of the appearance of Co^{4+} ions with localized electron spins in the deintercalated phases upon cobalt oxidation. Indeed, as already observed in the parent deintercalated Li_xCoO_2 system ($0.94 < x < 1.0$; $x_0 = 1.0$), the presence of such Co^{4+} ions in a diamagnetic Co^{3+} lattice

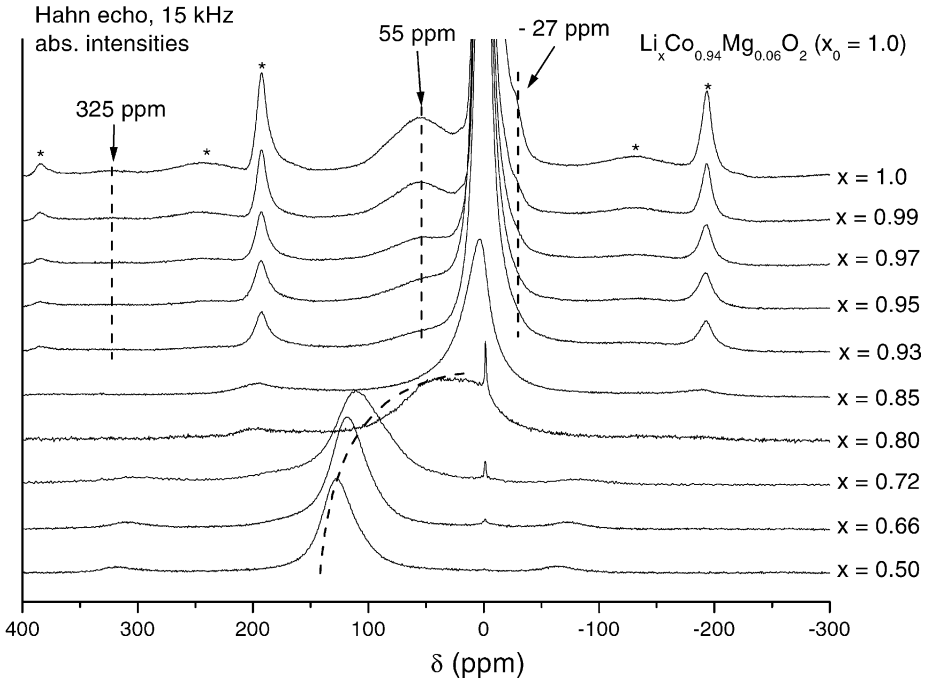

Fig. 7. ^{7}Li MAS NMR spectra for the various electrochemically deintercalated $Li_xCo_{0.94}Mg_{0.06}O_2$ ($x_0 = 1.0$) samples ($0.50 \leq x \leq 1.0$) (spinning speed = 15 kHz, ∗: spinning sidebands).

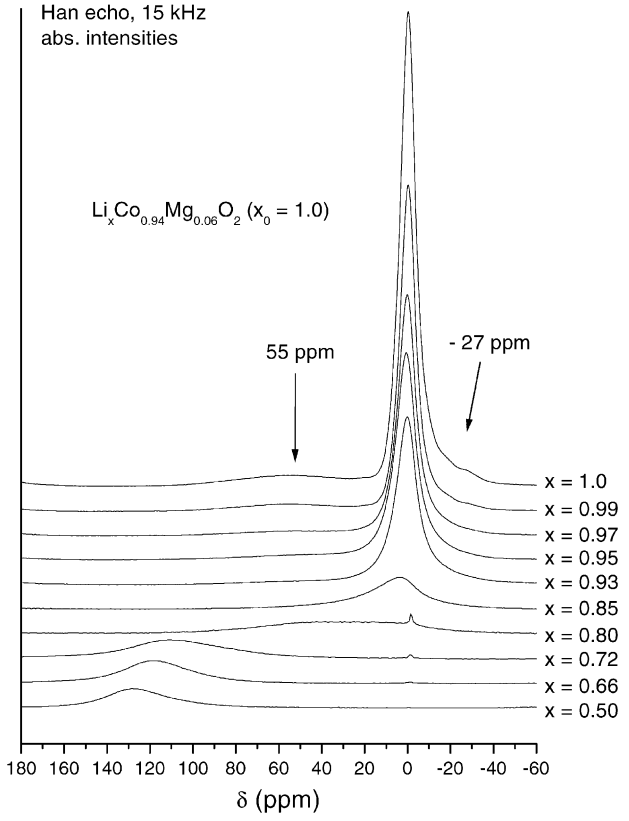

Fig. 8. Expansion of the central signal of 15 kHz ^{7}Li MAS NMR spectra for the various $Li_xCo_{0.94}Mg_{0.06}O_2$ ($x_0 = 1.0$) samples ($0.50 \leq x \leq 1.0$).

leads to a global loss of observability of the ^{7}Li MAS NMR signals due to a too strong directly transferred hyperfine interaction between Li^+ and the neighboring Co^{4+} t_{2g} single electron [22].

For $0.72 \leq x < 0.85$, a new signal grows at the expense of the 0 ppm one, the position of which shifts further upon deintercalation in the 40–120 ppm range. By analogy with the non-substituted Li_xCoO_2 ($x_0 > 1.0$) phases [32], we attribute this signal to a "Knight–Shift" type interaction due to a tendency toward electronic delocalisation which occurs in the material in small zones of the crystal, the structural defect preventing any long-scale electronic delocalisation, so that no phase separation takes place upon deintercalation.

For $x < 0.72$, the 0 ppm signal has disappeared and the new "Knight-Shifted" signal shifts further as the "metallic" character of the material increases.

3.2.2. $Li_xCo_{0.94}Mg_{0.06}O_2$ ($x_0 = 1.10$) materials

The ^{7}Li MAS NMR spectra of the various $Li_xCo_{0.94}Mg_{0.06}O_2$ ($x_0 = 1.10$) phases are shown in Figs. 9 and 10.

The pristine material indeed exhibits more intense 325 and −27 ppm signals related to the $Co^{3+(IS)}$ ion in the defect, whereas the 55 ppm signal is less well defined, due to lithium overstoichiometry as discussed in [16]. However, the general trend upon deintercalation is the same as that for $Li_xCo_{0.94}Mg_{0.06}O_2$ ($x_0 = 1.0$) described in Section 3.3. Indeed, one can observe a strong decrease of the global intensity due to the creation of Co^{4+} ions with localized electron spins upon charging. Upon deeper deintercalation, for $0.82 \leq x < 0.95$, a "Knight-Shifted" signal grows at the expense of the 0 ppm one, which arises from the existence of small metallic domains in the semi-conducting lattice. For $x < 0.82$, this new signal shifts further upon deeper oxidation of the cobalt ions, as the metallic character of the material increases.

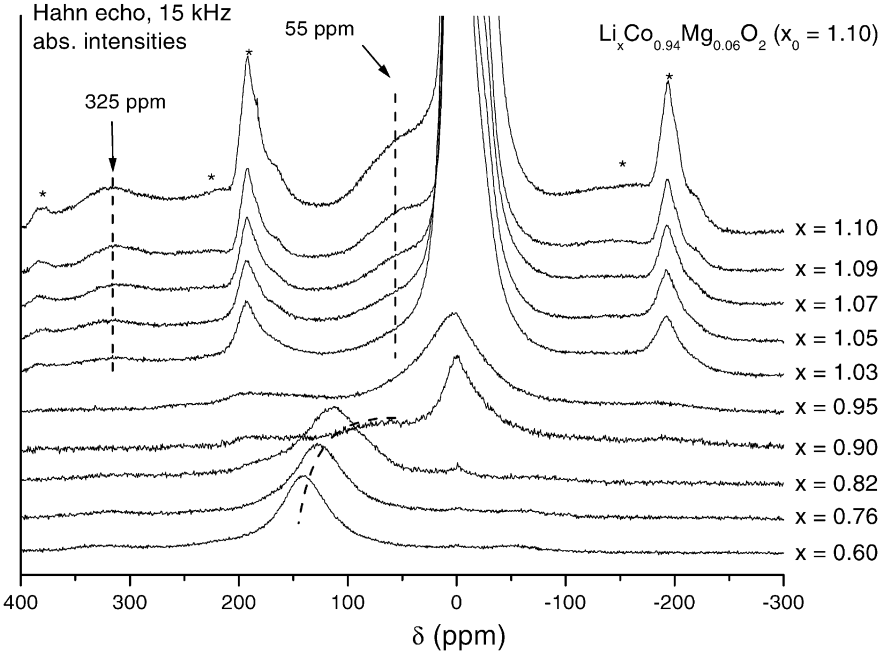

Fig. 9. ^{7}Li MAS NMR spectra for the various $Li_xCo_{0.94}Mg_{0.06}O_2$ ($x_0 = 1.10$) samples ($0.60 \leq x \leq 1.10$), (spinning speed = 15 kHz, ∗: spinning sidebands).

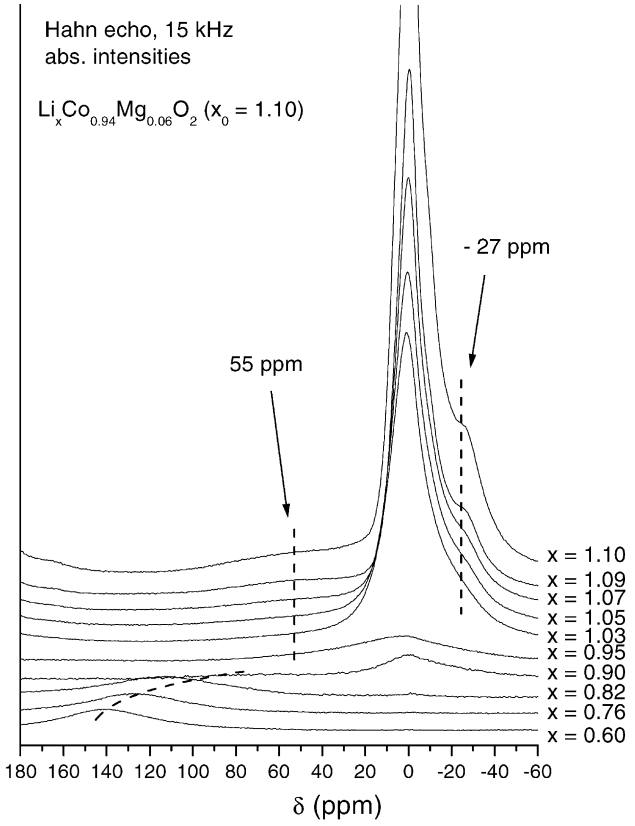

Fig. 10. Expansion of the central signal of 15 kHz ^{7}Li MAS NMR spectra for the various $Li_xCo_{0.94}Mg_{0.06}O_2$ ($x_0 = 1.10$) samples ($0.60 \leq x \leq 1.10$).

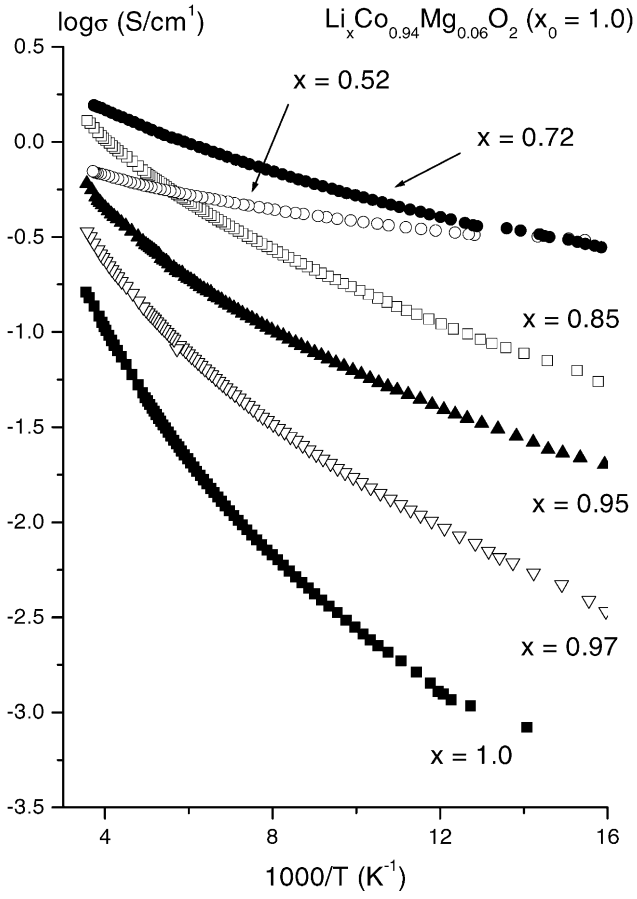

Fig. 11. Variation of the logarithm of the electrical conductivity vs. reciprocal temperature for the $Li_xCo_{0.94}Mg_{0.06}O_2$ ($x_0 = 1.0$; $0.50 \leq x \leq 1.0$) phases.

3.3. Electrical properties study

The ^{7}Li MAS NMR showed that the behavior upon deintercalation of the $Li_{x0}Co_{0.94}Mg_{0.06}O_2$ ($x_0 = 1.0$ and 1.10) is very similar, whatever the nominal Li/Co ratio used for the materials' preparation. As the measurements of the electrical properties confirm this similarity, only those from the $Li_xCo_{0.94}Mg_{0.06}O_2$ ($x_0 = 1.0$) phases will be discussed here.

3.3.1. Electronic conductivity measurements

Fig. 11 shows the variation of the electronic conductivity versus reciprocal temperature for the $Li_xCo_{0.94}Mg_{0.06}O_2$ ($x_0 = 1.0$) electrochemically deintercalated phases.

In all cases, a global semi-conducting behavior is evidenced as the dc conductivity remains thermally activated whatever the deintercalation amount. This can be explained by the fact that some Co^{4+} ions with localized electron spins are created at the beginning of the charge process, when oxidizing diamagnetic Co^{3+} ions, in good agreement with the ^{7}Li NMR results.

For $0.85 \leq x \leq 1.0$, the dc conductivity increases and the activation energy decreases suggesting an increase in the number of charge carriers. This result shows that the Co^{3+}/Co^{4+} hopping mechanism taking place in $Li_xCo_{1-y}Mg_yO_2$ systems ($y \geq 0$) upon lithium deintercalation allows to reach higher conductivity values than those obtained from the existence of small "metallic domains" located around Mg^{2+} ions and separated by poorly conducting zones in the $Li_{x0}Co_{1-y}Mg_yO_2$ phases.

One can note that the conductivity curve for the $Li_{0.52}Co_{0.94}Mg_{0.06}O_2$ ($x_0 = 1.0$) phase is almost independent of temperature, but does not show a real metallic behavior. Considering the ^{7}Li MAS NMR results, one can expect the $Li_{0.52}Co_{0.94}Mg_{0.06}O_2$ ($x_0 = 1.0$) phase to be metallic. The macroscopic semi-conducting behavior observed from the conductivity measurements could result from the presence of Mg^{2+} ions in the material which block the long-range electronic delocalisation; it could also be due to the fact that the value of the conductivity of sintered pellets is very sensitive to their compacity; in the case of electrochemically deintercalated materials, the change in the cell parameters leads to constraints and local loss of internal contacts which could further alter the conductivity values.

3.3.2. Thermopower measurements

Fig. 12 shows the variation of the thermoelectronic power data in the 75–300 K temperature range for the $Li_xCo_{0.94}Mg_{0.06}O_2$ ($x_0 = 1.0$) electrochemically deintercalated phases. The results shown here are comparable to those obtained in

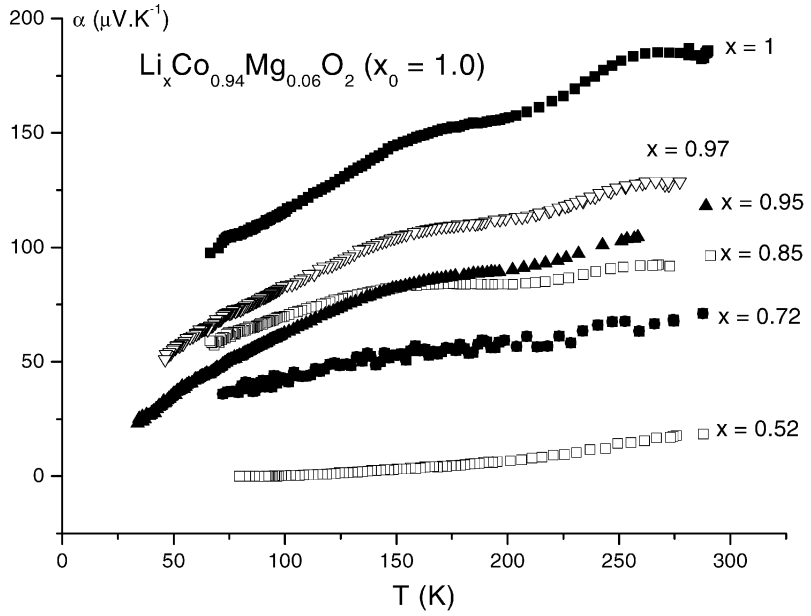

Fig. 12. Thermal variation of the Seebeck coefficient for the $Li_xCo_{0.94}Mg_{0.06}O_2$ ($x_0 = 1.0$; $0.50 \leq x \leq 1.0$) phases.

the case of non Mg-doped Li_xCoO_2 ($x_0 \geq 1.0$) materials [22,32]. In all cases, the positive value of the Seebeck coefficient evidences that electron holes are the main charge carriers in the $Li_xCo_{0.94}Mg_{0.06}O_2$ ($x_0 = 1.0$) phases. Indeed, as already observed by ^{7}Li NMR, as oxidation of LS Co^{3+} (t_{2g}^6) proceeds with lithium deintercalation, more and more Co^{4+} ions with one hole in the t_{2g} orbital (t_{2g}^5) are created.

The high values of the thermopower for $x = 1.0$ are typical of a semi-conductor behavior. For $0.85 \leq x < 1.0$, the decrease in the values of the thermoelectronic power reflects the increase of the number of charge carriers as oxidation of Co ions occurs in the $Li_xCo_{0.94}Mg_{0.06}O_2$ ($x_0 = 1.0$) phases. Finally, the linear $\alpha = f(T)$ curve for $x \leq 0.72$, and the low value of the Seebeck coefficient, which tends to zero when temperature decreases, is typical of a pseudo-metallic behavior, in very good agreement with the NMR results.

4. General discussion and conclusion

The present study confirms all the previous results by Tukamoto and West [14]. The overall good electrochemical behavior and the large reversibility of the $Li_{x0}Co_{1-y}Mg_yO_2$ phases, whatever y, could be explained by the existence of a solid solution upon lithium deintercalation, thus enhancing the structural stability upon cycling. This is fully confirmed by our XRD measurements which showed that the layered structure is retained after 60 cycles, no migration of the Mg^{2+} ions being evidenced. This set of results confirms that the Mg-doped $Li_{x0}Co_{1-y}Mg_yO_2$ phases are of interest from an applied point of view as positive electrode for Li-ion batteries.

In addition, the ^{7}Li MAS NMR study allowed us to point out the very peculiar behavior of the $Li_xCo_{1-y}Mg_yO_2$ phases upon lithium deintercalation. Indeed, despite the ''metallic'' character locally induced by the (formally) Co^{4+} ions generated by the substitution (sharing an itinerant electron hole with neighboring Co^{3+} ions), the oxidation upon lithium deintercalation do not start from these ''metallic domains'' around Mg^{2+} ions, but leads to the creation of Co^{4+} ions with localized electron spins. As a result, at the beginning of the oxidation process, the $Li_xCo_{1-y}Mg_yO_2$ phases exhibit a strong semi-conducting behavior, even if the global conductivity increases upon lithium deintercalation. For $x < 0.85$, like in the case of non Mg-doped Li_xCoO_2 ($x_0 = 1.10$) materials [32], one can observe a tendency to electronic delocalisation which starts only in small zones of the crystal, and consequently does not induce any structural transition upon lithium deintercalation. The similarity of the evolution upon lithium deintercalation of the $Li_{x0}Co_{1-y}Mg_yO_2$ phases, whatever x_0 on the one hand, and of the Li-overstoichiometric $Li_{x0}CoO_2$ ($x_0 > 1.0$) on the other hand suggests that this behavior is governed by the presence of the structural defect (O vacancy and $Co^{3+(IS)}$), regardless of the presence of Mg^{2+} ions in the structure.

Acknowledgements

The authors wish to thank A. Audemer, L. Gautier and J. Scoyer for fruitful discussions, E. Marquestaut and R. Decourt (for technical assistance with the electrical properties measurements), J. Hirschinger and B. Meurer (for the use of their NMR spectrometer) and Umicore, ANRT and Région Aquitaine for financial support.

References

[1] K. Mizushima, P.C. Jones, P.J. Wiseman, J.B. Goodenough, Mater. Res. Bull. 15 (1980) 783.
[2] H. Abe, K. Zaghib, K. Tatsumi, S. Higuchi, J. Power Sources 54 (1995) 236.
[3] H.J. Orman, P.J. Wiseman, Acta Cryst. C 40 (1984) 12.
[4] C. Delmas, I. Saadoune, A. Rougier, J. Power Sources 43-44 (1993) 595.
[5] I. Saadoune, C. Delmas, J. Mater. Chem. 6 (2) (1996) 193.
[6] A. Ueda, T. Ohzuku, J. Electrochem. Soc. 141 (8) (1994) 2010.
[7] S. Levasseur, M. Ménétrier, C. Delmas, J. Electrochem. Soc., in press.
[8] R. Stoyanova, E. Zhecheva, L. Zarkova, Solid State Ionics 73 (1994) 233.
[9] S. Waki, K. Dokko, T. Itoh, M. Nishizawa, T. Abe, I. Uchida, J. Solid State Electrochem. 4 (2000) 205.
[10] C.D.W. Jones, E. Rossen, J.R. Dahn, Solid State Ionics 68 (1994) 65.
[11] Y.I. Jang, B. Huang, H. Wang, G.R. Maslkaly, G. Ceder, D.R. Sadoway, Y.M. Chiang, H. Liu, H. Tamura, J. Power Sources 81-82 (1999) 589.
[12] G.A. Nazri, A. Rougier, C. Julien, Solid State Ionics 135 (2000) 121.
[13] H. Kobayachi, H. Shigemura, M. Tabuchi, H. Sakaebe, K. Ado, H. Kageyama, A. Hirano, R. Kanno, M. Wakita, S. Morimoto, S. Nasu, J. Electrochem. Soc. 147 (3) (2000) 960.
[14] H. Tukamoto, A.R. West, J. Electrochem. Soc. 144 (9) (1997) 3164.
[15] M. Carewska, S. Scaccia, S. Arumugam, Y. Wang, S. Greenbaum, Solid State Ionics 93 (1997) 227.
[16] S. Levasseur, M. Ménétrier, C. Delmas, Chem. Mater. 14 (2002) 3584.
[17] S. Levasseur, M. Ménétrier, Y. Shao-Horn, L. Gautier, A. Audemer, G. Demazeau, A. Largeteau, C. Delmas, Chem. Mater., submitted for publication.
[18] C. Pouillerie, L. Croguennec, C. Delmas, Solid State Ionics 132 (2000) 15.
[19] J. Rodriguez-Carvajal (Ed.), Proceedings of the Satellite Meeting on Powder Diffraction of the XV Congress of the IUCr, 1990, p. 127. http://www.11b.cea.fr/fullweb/powder.htm.
[20] P. Dordor, E. Marquestaut, G. Villeneuve, Revue Phys. Appl. 15 (1980) 1607.
[21] J.N. Reimers, J.R. Dahn, J. Electrochem. Soc. 139 (8) (1992) 2091.
[22] M. Ménétrier, I. Saadoune, S. Levasseur, C. Delmas, J. Mater. Chem. 9 (1999) 1135.
[23] Y. Shao-Horn, F. Weill, S. Levasseur, C. Delmas, J. Electrochem. Soc., submitted for publication.
[24] J.N. Reimers, J.R. Dahn, U. Von Sacken, J. Electrochem. Soc. 140 (10) (1993) 2752.
[25] C. Delmas, I. Saadoune, Solid State Ionics 53/56 (1992) 370.
[26] G. Prado, A. Rougier, L. Fournès, C. Delmas, J. Electrochem. Soc. 147 (8) (2000) 2880.
[27] J.R. Muellerneuhaus, R.A. Dunlap, J.R. Dahn, J. Electrochem. Soc. 147 (10) (2000) 3598.
[28] J. Kim, K. Amine, Electrochem. Commun. 3 (2001) 52.
[29] B.V.R. Chowdari, G.V. Subba Rao, S.Y. Chow, Solid State Ionics 140 (2001) 55.
[30] C.C. Chang, J.Y. Kim, P.N. Kumta, J. Electrochem. Soc. 147 (5) (2000) 1722.
[31] L. Croguennec, E. Suard, P. Willmann, C. Delmas, Chem. Mater. 14 (2002) 2149.
[32] S. Levasseur, M. Ménétrier, E. Suard, C. Delmas, Solid State Ionics 128 (2000) 11.